International Journal of Environment and Geoinformatics 10(4):017-025 (2023)

Research Article

Utilization of Bio-waste Mussel Shell as a Decoration Material on LiCoO2 Cathode.

Mehmet Emre Cetintasoglu[1], Ozgul Keles[2], Nuray Caglar Balkis[1]

[1] Department of Chemical Oceanography, Institute of Marine Science and Management, Istanbul University, Vefa, 34134, Istanbul, Türkiye
[2] Department of Metallurgical and Materials Engineering, Istanbul Technical University, Maslak, Istanbul, 34469, Türkiye

* Corresponding author: M. E. Çetintaşoğlu
E-mail: emre.cetintasoglu@istanbul.edu.tr

Received 28.09.2023
Accepted 13.10.2023

How to cite: Cetintasoglu, et al., (2023). Utilization of Bio-waste Mussel Shell as a Decoration Material on LiCoO2 Cathode, *International Journal of Environment and Geoinformatics (IJEGEO)*, 10(4):017-025. doi. 10.30897/ijegeo.1367737

Abstract

In this study, thermochemical conversion of mussel shells as biological waste utilizations has been made as a protection layer for cathode active materials. $LiCoO_2$ material synthesized via sol-gel method and coated with CaO produced using mussel shells. An appropriate coating ratio enhances the cycling performance with a better specific capacity (170 mAh g^{-1} at 1C). Surface modification plays a crucial role in attaining an improved performance of LCO by reducing its interference between electrolytes. This study present the use of biological waste mussel shell as decoration agent for cathode active materials and lead up to decrease the amount of biological wastes.

Keywords: Mussel shell, CaO, Lithium-ion batteries, biomaterials, waste to energy.

Introduction

In today's technology the use of lithium cobalt oxide (LCO) is still increasing in the electric vehicles, consumer electronics and telecommunications (Duh et al. 2021). However, its low practical capacity compared to other equivalent metal oxides reduce its potential usage in the expanding market due to increasing need for high energy density batteries. Even though LCO poses a high theoretical specific capacity (~270 mA h g^{-1}) only half of its capacity can be attained (~140 mAh/g when operated. at 3.9 V) Because, in case of high delithiation the fundamental structural instability and interfacial volatility between electrolyte and electrode occur. Thus, limiting to reach the needs for high energy density applications such as EVs (Li et al. 2020).

During the deintercalation process of lithium ions only half of the Li^+ from the $Li_{1-x}CoO_2$ ($0 \leq x \leq 0.5$) structure can be removed at 4.2 V (140 mAh/g). Charging the battery above the 4.2 V to remove more Li^+ from $LiCo_2O_4$ leads to anisotropic shrinkage of the rhombohedral a-$NaFeO_2$ type lattice in the *c*-direction because of the repulsive interactions among CoO_2 sheets (Verdier et al. 2007; Zhou et al. 2016). This structural degradation of LCO greatly reduce the cycling performance due to the strong escalation in Co dissolution in the electrolyte. Even though higher capacity values can be attained with the ascending charge cut-off voltage, the capacity retention of $LiCoO_2$ quickly dwindles. Thus, it is crucial to sustain the good cyclability while increasing the energy density in the large voltage window. On this subject, various procedures have been suggested for the cycling performance degradation of LCO, such as Co dissolution, electrolyte oxidation, and structural instability of highly de-lithiated LCO. To overcome these drawbacks, surface coating is a valuable strategy to enhance cycle performance of cathode materials. Metal-oxide coating such as ZnO (Shen et al. 2017), MgO, TiO_2 (Xiao et al. 2019), ZrO_2 (Takamatsu et al. 2013), and Al_2O_3 (Jian et al. 2018) proposing an encouraging improvement in discharge-capacity reversibility upon cycling by surpassing the electrode degradation. Moreover, with the stable layer shaped on the surface of the cathode materials, the dissolution of transition metals can be prevented, and this leads a stable structure with enhanced cyclic performance (Kaur et al. 2022). Compared to the materials used in surface coating, bio-based materials are abundant in nature, environmentally friendly and inexpensive to process. Among shellfish, mussels are the most consumed product, therefore they generate high amount of waste each year. As stated by the 2014 report of the The Food and Agriculture Organization of the United Nations (FAO), one-year usage of mussels was given as $6x10^5$ tons only in the European Union countries. Considering these data, millions of tons of mussel shells remain in nature as waste every year. It has been reported in another study that the use of mussel shells after recycling has a significant effect on reducing fluorite pollution in nature (Kochan, 2020). The main composition of the mussel shell is calcium carbonate ($CaCO_3$), but when heat treatment is applied at temperatures of 700 ^oC and above, $CaCO_3$ turns into calcium oxide (CaO) (Srichanachaichok et al. 2023). In this study, we take the advantage of the high chemical resistance of calcium oxide by modifying the surface of $LiCO_2$ particles to decrease the electrolyte-active material interaction, and for the first time an additive material produced from mussel shells is used as a coating agent for electrodes.

Table 1. CaO decoration parameters of $LiCoO_2$.

Sample Code	Surface Decoration	Decoration Method	Decoration Ratio (wt. %)
LCO	-	-	-
0.5*CG-LCO	*Chamelea gallinar*	Ball miller	0.5
1*CG-LCO	*Chamelea gallinar*	Ball miller	1
2*CG-LCO	*Chamelea gallinar*	Ball miller	2

In the work, we form CaO with different weight percentages on LCO particles by applying a thermochemical conversion to biological waste mussel shells, and the effect of CaO modification applied at different rates on the electrochemical and structural properties of LCO are examined in detail.

Materials and Methods

$LiCoO_2$ powder was produced via a sol–gel method. Lithium acetate dihydrate ($CH_3COOLi_2H_2O$), Co acetate tetrahydrate ($(CH_3COO)_2Co_4H_2O$) and citric acid were dissolved in ultra pure water with the Co:Li:citric acid (1:1:2) stoichiometry. The mixture pH is adjusted to 8.5 by adding NH_4OH solution. The attained gel is dried at 120 ºC for 12 h and then a twostep heat treatment is procured. Foremost to eliminate residual compounds, the obtained form was subjected to 550 ºC for 3 h. Then, the particles were exposed to 800 ºC for 8 h.

Chamelea gallina mussel shells are used as a $CaCO_3$ sources. The surface decoration of LCO is achieved by using ball miller and then followed by a calcination process. LCO particles that are synthesized via sol-gel route mixed with mussel shell powder and mechanically mixed at 800 rpm for 2 hours in air to attain fine powders of the $CaCO_3$ decorated LCO. The samples are decorated to LCO with 0.5, 1 and 2 wt% CaO and abbreviated as 0.5%CaO-LCO, 1%CaO-LCO and 2%CaO-LCO (Table 1). Lastly, heat treatment procedure is applied to ball-milled samples at 400 ºC for 2 hours and 800 ºC for 6 hours to obtain CaO decorated LCO.
Morphological features are imaged by scanning electron microscope (SEM). The phase purity and crystal structure of synthesized materials are examined by XRD instrument (Rigaku) at 2θ =10°–90° with the scanning speed of 2°/min.

The FTIR spectra of samples are procured via KBr method (Perkin Elmer) at room temperature and the spectra are analyzed at 400-4000 cm^{-1}.

The cathode consists of CaO-LCO as an active material, polyvinylidene difluoride (PVDF) as a polymeric binder, and carbon black as a conductive agent in the respective wt.% ratio 80:10:10. N-methylpyrrolidinone (NMP) is used to dissolve PVDF, and then the carbon black and active material are added under stirring. The slurry is coated on a current collector (Al foil) and dried overnight at 120 ºC in a vacuum oven. The cathode is pressed via manual rolling press machine. To measure electrochemical peformances, CR2032 half-cells are gathered in an Argon containing glove box. As an electrolyte 1 M $LiPF_6$ (TOB Machine) in ethylene carbonate / dimethyl carbonate (1:1 by wt.%) is used, a polypropylene membrane is selected as a separator and lithium metal is used as a counter electrode.

Galvanostatic discharge/charge tests are procured in a voltage range of 3.0 – 4.3V using a battery analyzer (BST8-WA2 battery tester). C-rate analyses are carried out between 0.1C and 5C. The electrochemical impedance spectroscopy (EIS) of the electrode is executed at GAMRY potentiostat in the frequency band from 1 MHz to 100 kHz. Cyclic voltammetry (CV) analysis are evaluated between 3.0 and 4.3V and the scan rate is set to 0.03 mV/s.

Results and Discussion

The FTIR spectra of *Chamelea gallina* mussel shells and CaO obtained from thermal conversion are shown in Figure 1. The raw shell displayed spectral FTIR bands associated to $CaCO_3$. As the mussel shells dried at 110 ºC before the FT-IR analyses there is no broad transmission peak observed due to the -OH stretching vibration from water. Sharp peaks at 1415, 875 and 713 cm^{-1} are specific peaks of bending modes of $CaCO_3$ and C-O stretching and specifies the existence of $CaCO_3$ (Margaretha et al. 2012). After the heat treatment all those peaks disappeared. The sharp peak at 3637 cm^{-1} is related with OH stretching vibration on the surface of the calcium oxide. Additionally, broad peaks of CaO occurred at around 1415 cm^{-1} and 829 cm^{-1} (Hussein et al. 2020).

Small peaks between 1300 cm^{-1} and 800 cm^{-1} in the FT-IR analysis of LCO (Figure 2) correspond to the CH_2 and CO bands brought by the citric acid used during the synthesis. The absorption bands at 670 cm^{-1} represent the vibration on octahedral CoO_4, while the vibration at 525 cm^{-1} belongs to tetrahedral LiO_4 (Wang et al. 2005).

Layered LCO has two octahedral and four tetrahedral sites, with both the Co and Li ions occupying the octahedral sites (Ong et al. 2011). The Li layers standing between slabs of octahedrons shaped by oxygen and cobalt ions (He et al. 2012). XRD is used to characterize the LCO to verify the crystal structure of the sample and the diffraction peaks are given in Figure 3a. Synthesized LCO matched with the reference pattern (PDF 00-016-0427), which has rhombohedral symmetry ($R\bar{3}m$) (Johnston et al. 1958). The LCO material that is calcined at 800 show characteristic peaks of LCO at 19.68°, 37.34°, 39.65°, 45.38°, 49.64°, 59.28°, 65.78°, 66.19°and 69.84°, corresponding to (003), (101), (012), (104), (015), (107), (108), (110) and (113) planes, respectively. A

minor impurity peak is also detected at 36.8° which can be attributed to Co_3O_4, a common impurity phase from LCO production. This Co_3O_4 phase likely caused from the unfinished lithium insertion of the $LiCoO_2$ material (Lin et al. 2022).

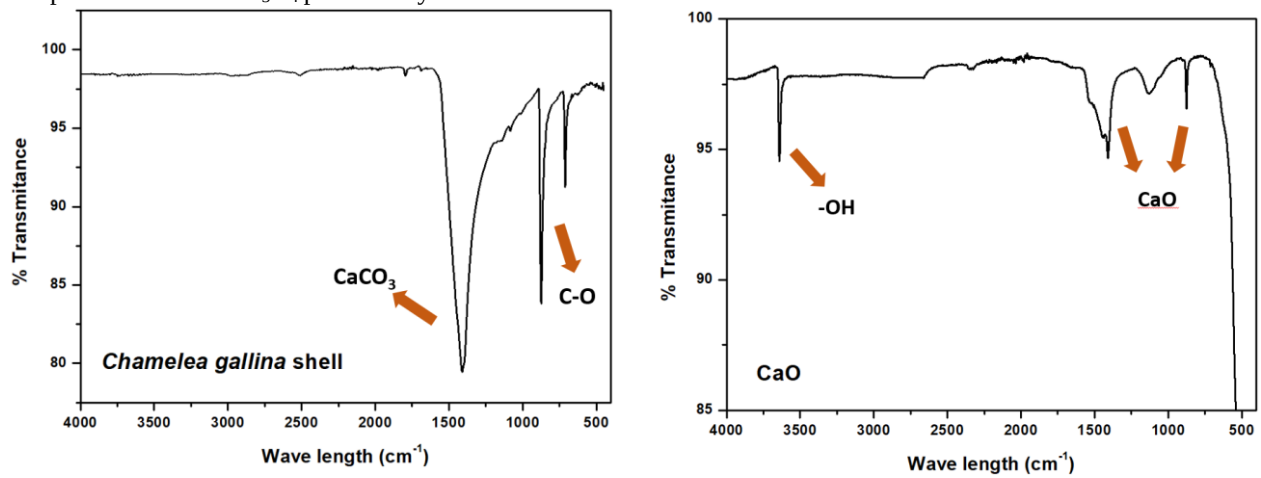

Fig. 1. FT-IR results of a) *Chamelea gallina* shell, b) CaO powder.

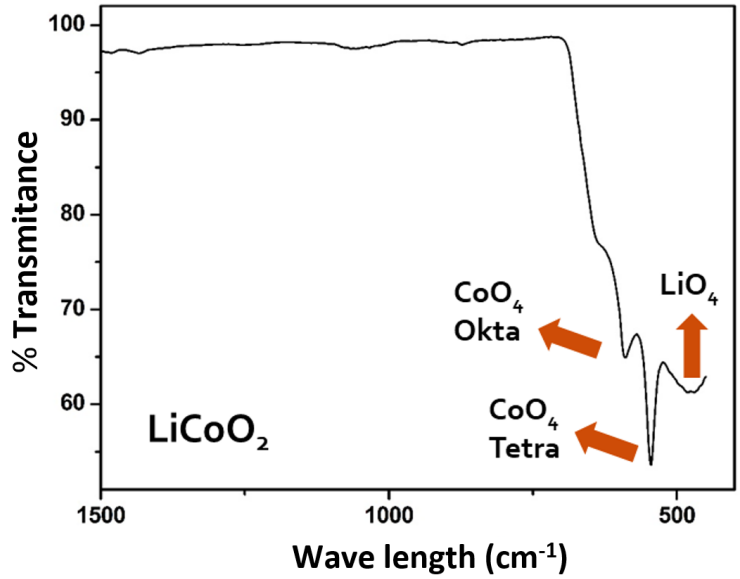

Fig. 2. FT-IR results of synthesized $LiCoO_2$ powder.

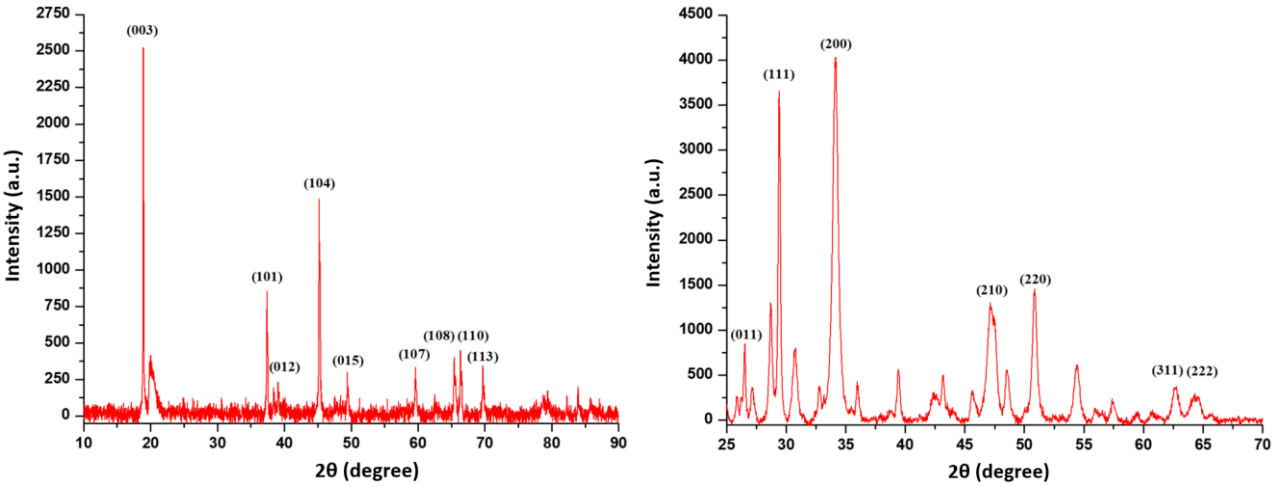

Fig.3. XRD spectrums of a) synthesized $LiCoO_2$ powder, b) thermochemically converted CaO powder.

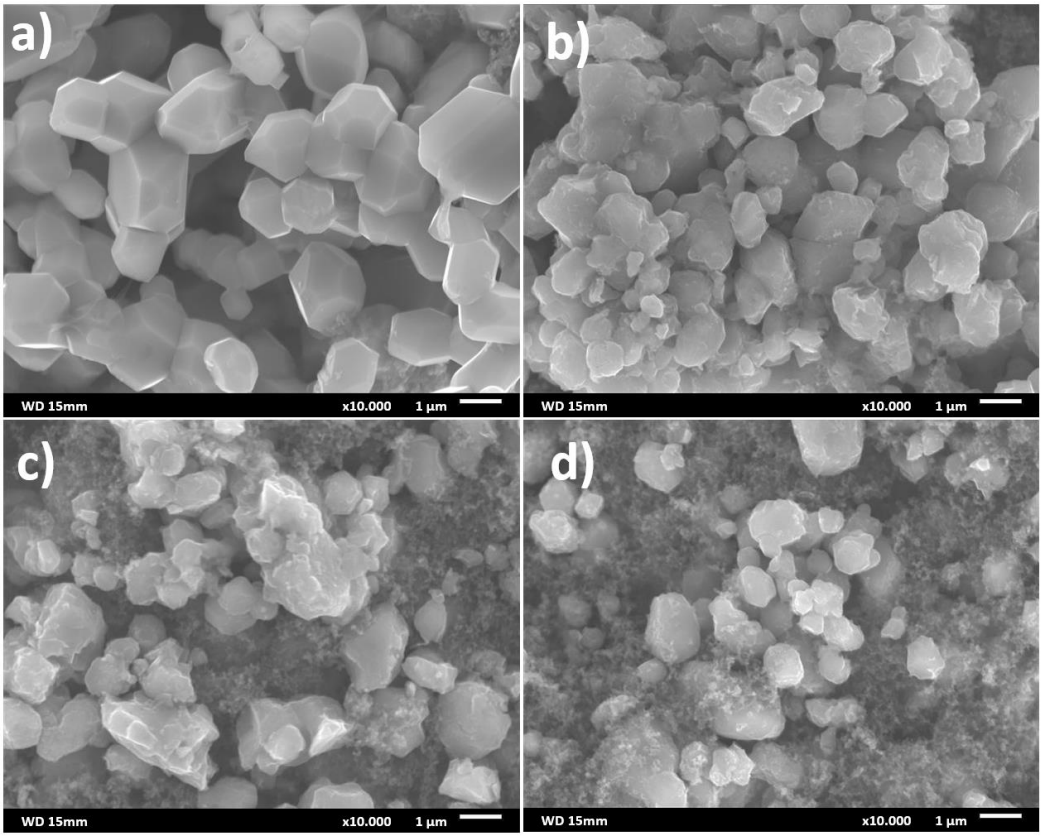

Fig. 4. SEM images of a) bare LCO, b) 0.5%CaO-LCO, c) 1%CaO-LCO, d) 2%CaO-LCO electrodes.

The XRD patterns demonstrate distinctive peaks of CaO particles at 26,51°, 29,41°, 34,22°, 47,19°, 50,91°, 62,68° and 64,43° relating to (011), (111), (200), (210), (220), (311) ve (222) planes of calcium oxides cubic system (Fig. 3b). The plane values of XRD patterns match with calcium oxide (JCPDS card No. 00-004-0777) with cubic crystal system. All obtained peak intensities are features of the cubic structure and the (002) peak shows anisotropic growth and indicates a preferred orientation of the crystallites. The narrow and stiff diffraction peaks imply that the CaO has a high crystallinity and there is no shift in the diffraction peaks (Jadhav et al. 2022). Figure 4 demonstrates the SEM patterns for bare LCO (a) and CaO decorated LCO powders (b, c, d). The scanning electron microscopy (SEM) patterns of bare and CaO-decorated LCO (Figure 4) show that particle size diverges between 400 and 1500 nm. In Figure 4a, particles have smooth surfaces and sharp edges but after ball milling process for 2 hours, all decorated particles attained soft edges with rough surfaces. Additionally, in Figure 4b–d, particles have become smaller after ball milling process for all decorated electrodes compared to the bare sample where the particle size varies between 1000 and 3000 nm. It is affirmed that the LCO surfaces decorated with CaO particles causing in rough surfaces, which are also experienced by other studies (Chen et al. 2015). In addition to this, milling process have caused an effect on the particle shape and size. SEM images displayed that ball milling is exceptionally effective in reducing the particle size. Related outcomes have also been stated for various cathode active materials ($LiFePO_4$, $LiCoO_2$, $LiNi_{0.6}Co_{0.2}Mn_{0.2}O_2$) (Chen et al 2014; Hu et al. 2019; Zhao et al. 2020).

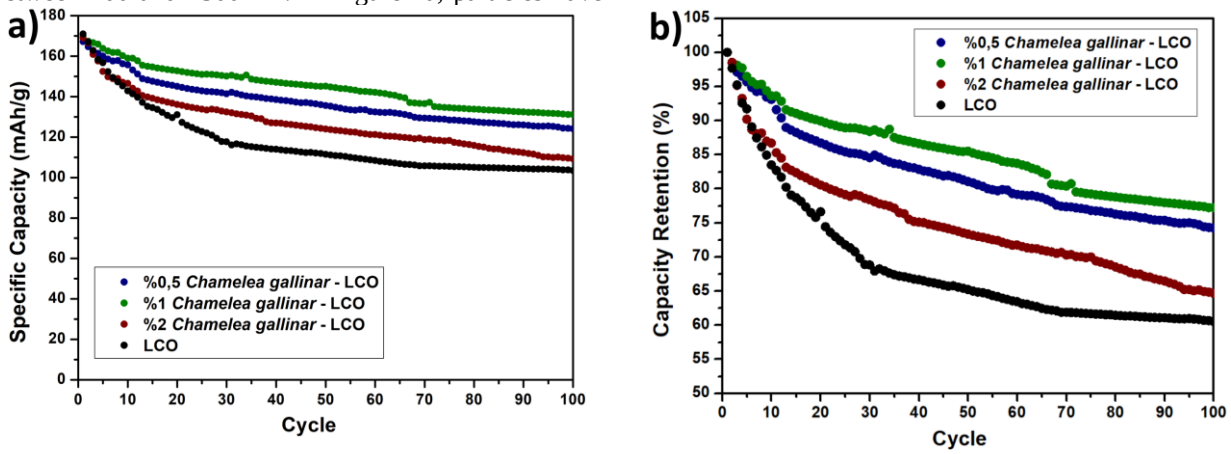

Figure 5. a) Specific capacity-cycle, b) Capacity retention-cycle graphics for all samples.

In Figure 5a, specific capacity-cycle curves of all samples are given comparatively and the electrochemical performance of various CaO decoration ratios on LCO are investigated. The first discharge capacity of bare LCO, 0.5%CaO-LCO, 1%CaO-LCO and 2%CaO-LCO electrodes at 0.2 C are 170.9, 167.2, 169,8, 169 mAh g^{-1} and their related capacity retentions at 100th cycle are 60.5%, 74,2%, 77.2% and 64.6%, respectively. Although bare LCO demonstrates a decent initial discharge capacity, it undergoes rapid fading. The explanation behind this fast capacity fading, which is also one of the common disadvantages for transition metal oxide cathodes, is the dissolution of Co^{+} ions in the existence of hydro fluoric acid that arose from $LiPF_6$ based electrolyte. This phenomenon causes a fast capacity fade throughout the cycling. The possible reaction mechanism for Co dissolution are stated in equations (1-3).

$$LiPF_6 \rightarrow PF_5 + LiF \qquad \text{(Eq.1)}$$

$$PF_5 + H_2O \rightarrow PF_3O + 2HF \qquad \text{(Eq. 2)}$$

$$LiCoO_2 + 4HF \rightarrow CoF_4 + Li^{+} + 2H_2O \qquad \text{(Eq.3)}$$

The correlation between the amount of cobalt separated from the metal oxide structure and the capacity loss has been revealed by different studies (Radin et al. 2017). With the separation of lithium ions from the LCO structure, Co^{3+} ions oxidize into the unstable Co^{4+} form. The formation of the high amount of Co^{4+} ions disrupts the crystallinity of the cathode structure and causes cobalt ions to dissolve in the electrolyte. These irreversible reactions cause the loss of the transition metals in the cathode structure and prepare the environment for the formation of interfacial side reactions (Reimers et al. 1992; Yu et al. 2018). The phase change from O3 to H1-3 occurs with the increase of the voltage, resulting in a significant shrinkage in the c-lattice parameter of the bulk $LiCoO_2$. Accordingly, there is a decrease in the diffusion of lithium ions, which leads to an increase in the concentration gradient and internal strains. After these irreversible phase transformations, the mechanical features of the LCO crystallites deteriorate and limit the use of LCO particles (Xia et al. 2007; Radin et al. 2017). The reason for applying CaO decoration to the LCO surface is to prevent the Co^{4+} ions loss by reducing the effect of the corrosive environment and parasitic reactions. The electrochemical reaction represented for the decorated CaO-LCO is given in Eq.4,

$$CaO + 2HF \rightarrow CaF_2 + H_2O \qquad \text{(Eq.4)}$$

As seen in Figure 5b, especially in 0.5%CaO-LCO, 1%CaO-LCO samples, reducing the contact of LCO with the electrolyte and preventing the formation of side reactions to a certain extent, resulting in higher capacity retention rates. However, at 2%CaO-LCO sample, it is observed that the capacity retention values decrease due to the ascending impedance and polarization in the structure, which will be further assisted by the subsequent EIS results.

Figure 6 is the initial charge/discharge curves of bare and decorated LCO's. Voltage plateau due to phase transformation during charge at high voltage (>4.5V) was not observed in any sample. Plateau seen during charge process imply the O3 + H1-3 phase and because of lower cut-off voltage (4.3V) the H1-3 + O1 phase peak was not observed in any active materials. Thus, oxygen loss at high voltages was prevented. To identify the diversity in capacity retention relating the decorated cathodes and bulk LCO, electrochemical impedance analyses are examined after 1st and 50th cycles at 3.0V over a frequency band from 100 kHz to 1 MHz. In Figure 7 the Nyquist plot of all samples for their first cycle are demonstrated. The solvent resistance (Rs) is implied by the shift of impedance at Z_0 axis. Resistance of surface (Rsf) is represented by the semicircle at high frequency section and indicates the solid electrolyte interphase (SEI) and CaO decoration. The sloping line in low frequency regions denotes the solid-state diffusion of Li-ions (W) and charge transfer resistance (Rct) in the LCO material (Bai et al. 2007). The fitted equivalent circuit for all plots is showed in Figure 8 and the data calculated from related equivalent circuit are presented in Table 2.

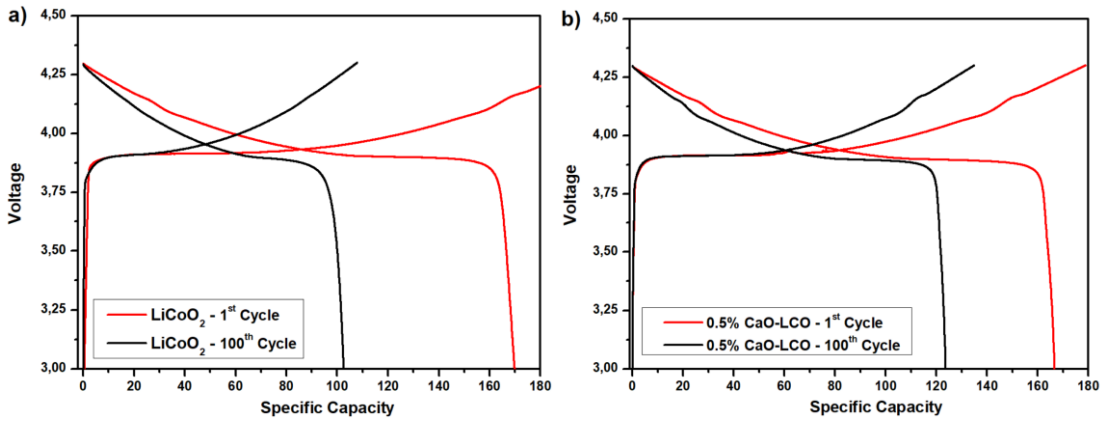

Fig. 6. Specific capacity-voltage graphics of a) bare LCO, b) 0.5%CaO-LCO, c) 1%CaO-LCO, d) 2%CaO-LCO for 1st and 100th cycles.

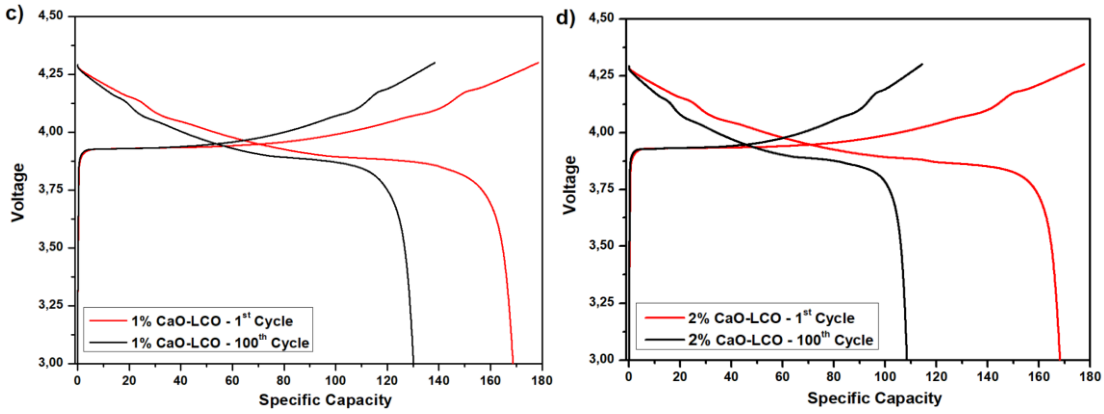

Fig. 6 (Cont.). Specific capacity-voltage graphics of a) bare LCO, b) 0.5%CaO-LCO, c) 1%CaO-LCO, d) 2%CaO-LCO for 1st and 100th cycles.

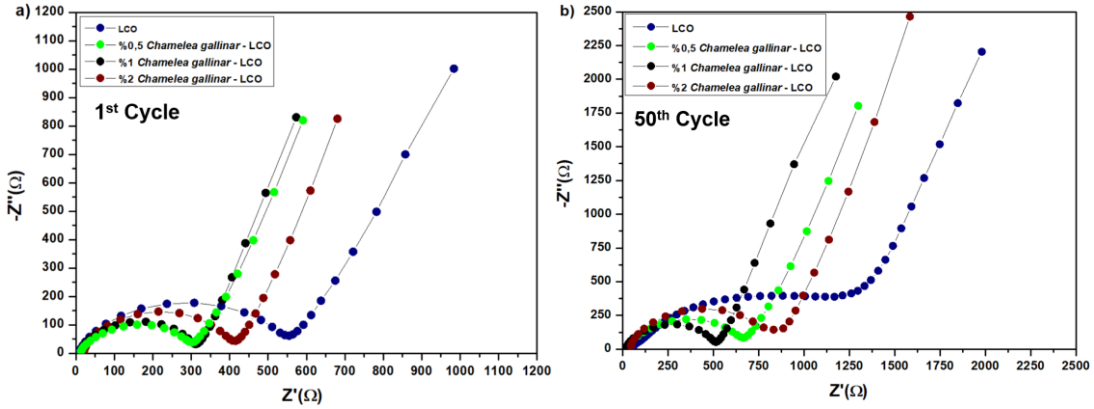

Fig. 7. Nyquist graphics of a) bare LCO, b) 0.5%CaO-LCO, c) 1%CaO-LCO, d) 2%CaO-LCO for 1st and 50th cycles.

The initial cycle calculations indicated that the bare LCO has higher surface resistance (Rsf) and charge transfer resistance (Rct). Although the LCO surfaces are decorated with non-conductive CaO, the main reason for obtaining lower impedance values than the decorated samples are thought to be due to the reduction of $LiCoO_2$ particle sizes during the grinding process used in the decoration of CaO (Zhao et al. 2020). Therefore, higher lithium diffusion through $LiCoO_2$ surface and lesser Rsf value are attained owing to the increase of the contact area between LCO surface and electrolyte.

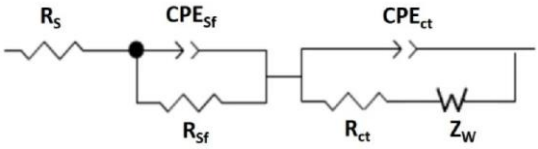

Fig. 8. Corresponding equivalent circuit of all samples.

In table 2, after 50 cycles CaO-decorated particles showed minor differences in the Rsf, whereas bare LCO demonstrated a noteworthy increase in Rsf. These outcomes denote that CaO decoration could decrease the interaction between the electrode and electrolyte and lessening the evolution of unsought SEI layer, which result in a more stable interface through cycling (Zhao et al. 2010). Additionally, the Rct of the bare LCO after 50 cycles is much greater than that of all the CaO decorated particles, causing in a better diffusion of Li-ions in electrode. The obtained outcomes specify that the CaO decoration can noticeably improve the kinetics of Li-ions diffusion throughout the ongoing cycles.

The outcomes of the above-mentioned EIS results are also observed clearly in C-rate analysis. The data imply that all CaO decorated LCO particles demonstrate higher discharge capacities compared to bare LCO at high C-rates. This shows that CaO decoration successfully improves the rate performance of LCO. And, between the all decorated electrodes 1%CaO-LCO displays slightly better C-rate result. Likewise, the discharge capacity completely restored once the C-rate is set to 0.2C, denoting that CaO-decorated LCO electrode has increased electrochemical reversibility and structural stability than bare LCO. However, when the surface decoration rate reaches %2, it is seen that the increased charged transfer resistance in the electrode affects the C-rate performance negatively. The electrochemical cycling results of LCO has been examined by exposing $LiCoO_2$/Li half cells to cyclic voltammetry studies (Figure 9). In the potential range of 2.9~4.2 V two meaningful oxidation peaks (4.02 and 4.17 V) are noted with corresponding reduction peaks (4.18, 4.07 and 3.84 V) for the initial cycle. A slight polarization can be visibly seen in the curves, corresponding to the phase transition relating the two O3 phases (Reimers et al. 1992; Chen et al. 2002). Likewise, highly distinct redox peaks at 3.97 and 4.16 for cathodic side and 3.78, 4.02 and 4.17 V are spotted for the same after completing 50 cycles, wherein a slight shift is detected in peak position due to the polarization increase through the cycles (Hu et al. 2021).

Table 2. Rs, Rsf and Rct results of the electrodes at 1st and 50th cycle on an equivalent circuit of the cell.

Sample Code	1st Cycle (Ω cm²)			50th Cycle (Ω cm²)		
	Rs	Rsf	Rct	Rs	Rsf	Rct
LCO	21.85	1009.15	982.79	64	2340.05	1368.22
0.5%CaO-LCO	23.33	604.66	574.48	58.32	1322.78	1292.73
1%CaO-LCO	24.6	628.08	510.75	41.63	1020.33	1340.25
2%CaO-LCO	29.49	830.05	534.71	73.58	1666.12	1516.43

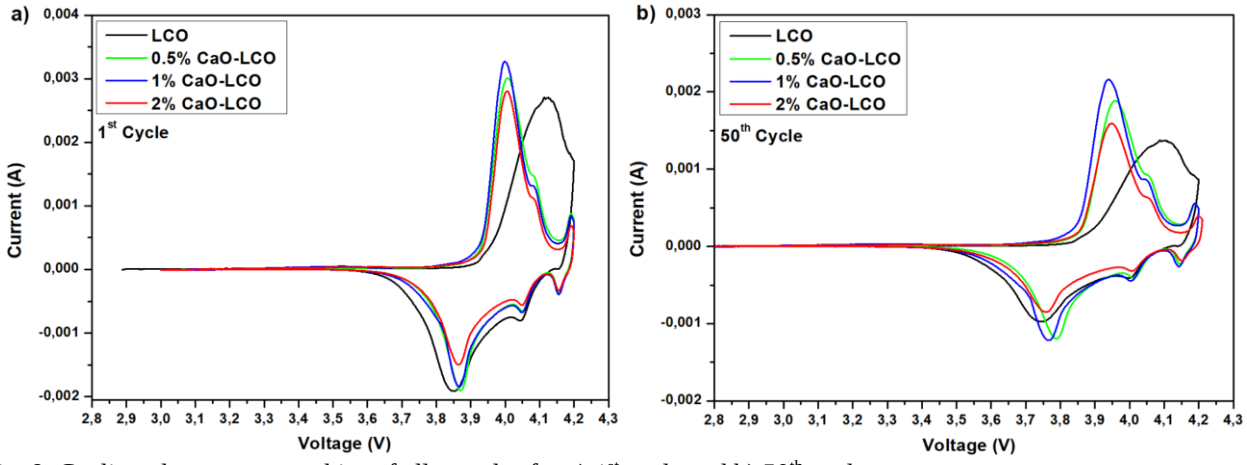

Fig. 9. Cyclic voltammetry graphics of all samples for a) 1st cycle and b) 50th cycle.

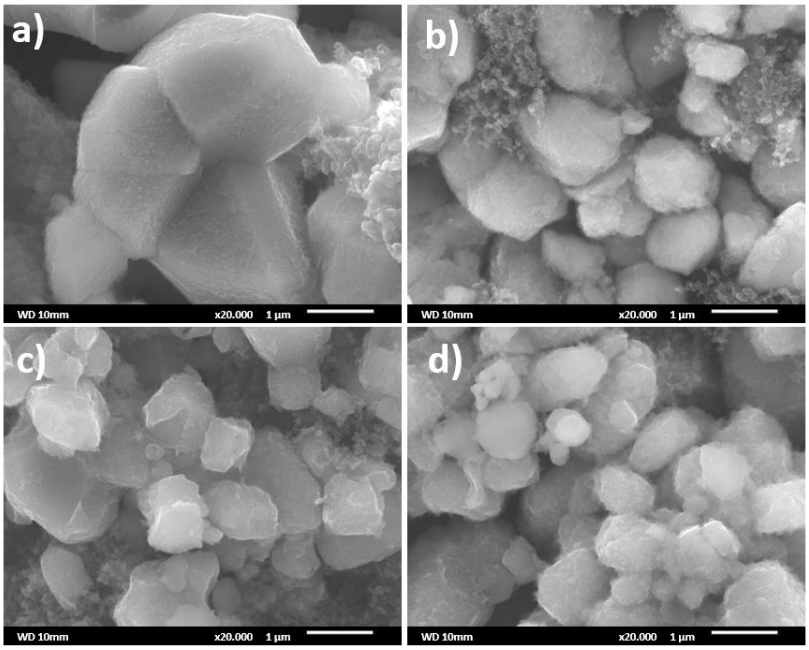

Fig. 10. SEM images of a) bare LCO, b) 0.5%CaO-LCO, c) 1%CaO-LCO, d) 2%CaO-LCO after 100th cycle.

SEM images after 100 cycles verified that particle morphology is well preserved and there are no visible cracks detected on the edge of LCO particles (Figure 10). The right amount of CaO decoration can thwart the side reactions and preserve the intercalation and deintercalation of lithium ions in and out of LCO lattice. Moreover, CaO layer can also provide decent mechanical properties by elastically shrink and expand simultaneously with LCO lattices through the intercalation and deintercalation processes, therefore extending the cycle life (Jian et al. 2018).

Conclusion

LCO particles are synthesized via sol–gel procedure. Then, CaO decoration on the particles from waste mussel shells is successfully applied via ball miller. Thermochemical conversion to biological waste mussel

shells to CaO provided better cycling performance compared to bare LCO. Electrochemical results showed that the first discharge capacity of the bare LCO electrode is 170.9 mAh/g and only 103.4 mAh/g could be retained (60.5% capacity retention) after 100 cycles. Comparatively, all the CaO-decorated electrodes have displayed improved rate performances and capacity retentions. 1%CaO-LCO cathode shows the best cycling performance amongst the other CaO coated samples at room temperature by 77.2% capacity retention and 129.1 mAh/g at 100 cycles.

Acknowledgements

The authors thank Scientific Research Projects Unit of Istanbul University for their supports to FDK-2019-35177 numbered project about this study.

References

Bai, Y., Yin, Y., Liu, N., Guo, B., Shi, H., Liu, J., Chen, L. (2007). New concept of surface modification to $LiCoO_2$. *Journal of power sources*, 174(1), 328-334.

Chen, G., Geng, H., Wang, Z., Yang, R., Xu, Y. (2016). On electrochemistry of Al_2O_3-coated $LiCoO_2$ composite cathode with improved cycle stability. *Ionics*, *22*, 629-636.

Chen, Y., Zhang, Y., Wang, F., Wang, Z., & Zhang, Q. (2014). Improve the structure and electrochemical performance of $LiNi_{0.6}Co_{0.2}Mn_{0.2}O_2$ cathode material by nano-Al_2O_3 ultrasonic coating. Journal of Alloys and Compounds, 611, 135-141.

Chen, Z., Lu, Z., Dahn, J. R. (2002). Staging phase transitions in Li_xCoO_2. *Journal of the Electrochemical Society*, 149(12), A1604.

Duh, Y. S., Sun, Y., Lin, X., Zheng, J., Wang, M., Wang, Y., Yu, G. (2021). Characterization on thermal runaway of commercial 18650 lithium-ion batteries used in electric vehicles: A review. *Journal of Energy Storage*, 41, 102888.

He, P., Yu, H., & Zhou, H. (2012). Layered lithium transition metal oxide cathodes towards high energy lithium-ion batteries. *Journal of Materials Chemistry*, 22(9), 3680-3695.

Hu, X., Yang, W., Jiang, Z., Huang, Z., Wang, Y., Wang, S. (2021). Improving diffusion kinetics and phase stability of $LiCoO_2$ via surface modification at elevated voltage. *Electrochimica Acta*, 380, 138227.

Hussein, A. I., Ab-Ghani, Z., Che Mat, A. N., Ab Ghani, N. A., Husein, A., Ab. Rahman, I. (2020). Synthesis and characterization of spherical calcium carbonate nanoparticles derived from cockle shells. Applied Sciences, 10(20), 7170.

Jadhav, V., Bhagare, A., Wahab, S., Lokhande, D., Vaidya, C., Dhayagude, A., Dutta, M. (2022). Green synthesized calcium oxide nanoparticles (CaO NPs) using leaves aqueous extract of moringa oleifera and evaluation of their antibacterial activities. *Journal of Nanomaterials*, 2022, 1-7.

Jian, Z., Wang, W., Wang, M., Wang, Y., AuYeung, N., Liu, M., Feng, Z. (2018). Al_2O_3 coated $LiCoO_2$ as cathode for high-capacity and long-cycling Li-ion batteries. *Chinese Chemical Letters*, 29(12), 1768-1772.

Johnston, W. D., Heikes, R. R., Sestrich, D. (1958). The preparation, crystallography, and magnetic properties of the $Li_xCo_{(1-x)}O$ system. *Journal of Physics and Chemistry of Solids*, 7(1), 1-13.

Kaur, G., Gates, B. D. (2022). Surface Coatings for Cathodes in Lithium Ion Batteries: From Crystal Structures to Electrochemical Performance. *Journal of The Electrochemical Society*, 169(4), 043504.

Kochan, C. (2020). An experimental investigation on mode-I fracture toughness of mussel shell/epoxy particle reinforced composites. *Pamukkale Universitesi Muhendislik Bilimleri Dergisi*, 26(4), 599-604.

Li, M., Lu, J. (2020). Cobalt in lithium-ion batteries. *Science*, 367(6481), 979-980.

Lin, J., Wu, J., Fan, E., Zhang, X., Chen, R., Wu, F., Li, L. (2022). Environmental and economic assessment of structural repair technologies for spent lithium-ion battery cathode materials. *International Journal of Minerals, Metallurgy and Materials*, 29(5), 942-952.

Margaretha, Y. Y., Prastyo, H. S., Ayucitra, A., Ismadji, S. (2012). Calcium oxide from Pomacea sp. Shell as a catalyst for biodiesel production. *International Journal of Environmental Engineering*, 3, 33–41.

Ong, S. P., Chevrier, V. L., Hautier, G., Jain, A., Moore, C., Kim, S., Ceder, G. (2011). Voltage, stability and diffusion barrier differences between sodium-ion and lithium-ion intercalation materials. *Energy & Environmental Science*, 4(9), 3680-3688.

Radin, M. D., Hy, S., Sina, M., Fang, C., Liu, H., Vinckeviciute, J., Van der Ven, A. (2017). Narrowing the gap between theoretical and practical capacities in Li-ion layered oxide cathode materials. *Advanced Energy Materials*, 7(20), 1602888.

Reimers, J. N., Dahn, J. R. (1992). Electrochemical and in situ X-ray diffraction studies of lithium intercalation in Li_xCoO_2. *Journal of the Electrochemical Society*, 139(8), 2091.

Shen, B., Zuo, P., Li, Q., He, X., Yin, G., Ma, Y., Gao, Y. (2017). Lithium cobalt oxides functionalized by conductive Al-doped ZnO coating as cathode for high-performance lithium ion batteries. *Electrochimica Acta*, 224, 96-104.

Srichanachaichok, W., Pissuwan, D. (2023). Micro/Nano Structural Investigation and Characterization of Mussel Shell Waste in Thailand as a Feasible Bioresource of CaO. *Materials*, 16(2), 805.

Takamatsu, D., Mori, S., Orikasa, Y., Nakatsutsumi, T., Koyama, Y., Tanida, H., Ogumi, Z. (2013). Effects of ZrO_2 coating on $LiCoO_2$ thin-film electrode studied by in situ X-ray absorption spectroscopy. *Journal of The Electrochemical Society*, 160(5), A3054.

Verdier, S., El Ouatani, L., Dedryvère, R., Bonhomme, F., Biensan, P., Gonbeau, D. (2007). XPS study on Al_2O_3- and $AlPO_4$-coated $LiCoO_2$ cathode material for high-capacity Li ion batteries. *Journal of The Electrochemical Society*, 154(12), A1088.

Wang, G. X., Yang, L., Chen, Y., Wang, J. Z., Bewlay, S., Liu, H. K. (2005). An investigation of polypyrrole-$LiFePO_4$ composite cathode materials for lithium-ion batteries. *Electrochimica Acta*, 50(24), 4649-4654.

Xia, H., Lu, L., Meng, Y. S., Ceder, G. (2007). Phase transitions and high-voltage electrochemical behavior of $LiCoO_2$ thin films grown by pulsed laser deposition. *Journal of The Electrochemical Society*, 154(4), A337.

Xiao, B., Wang, P. B., He, Z. J., Yang, Z., Tang, L. B., An, C. S., Zheng, J. C. (2019). Effect of MgO and TiO_2 Coating on the Electrochemical Performance of Li-Rich Cathode Materials for Lithium-Ion Batteries. *Energy Technology*, 7(8), 1800829.

Yu, X., Manthiram, A. (2018). Electrode–electrolyte interfaces in lithium-based batteries. *Energy & Environmental Science*, 11(3), 527-543.

Zhao, J., Wang, L., He, X., Wan, C., Jiang, C. (2010). Kinetic investigation of $LiCoO_2$ by electrochemical impedance spectroscopy (EIS). *International Journal of Electrochemical Science*, 5(4), 478-488.

Zhao, S., Zhang, W., Li, G., Zhu, H., Huang, J., He, W. (2020). Ultrasonic renovating and coating modifying spent lithium cobalt oxide from the cathode for the recovery and sustainable utilization of lithium-ion battery. *Journal of Cleaner Production*, 257, 120510.

Zhou, A., Xu, J., Dai, X., Yang, B., Lu, Y., Wang, L., Li, J. (2016). Improved high-voltage and high-temperature electrochemical performances of $LiCoO_2$ cathode by electrode sputter-coating with Li_3PO_4. *Journal of Power Sources*, 322, 10-16.